

# Modification of back electrode structure by a Mo intermediate layer for flexible CZTS thin film solar cells

Bo Long<sup>1</sup>, Shuying Cheng<sup>2</sup> ✉, Chuang Yue<sup>3</sup>, Limei Dong<sup>2</sup>

<sup>1</sup>College of Mechanical and Electrical Engineering, Fujian Agriculture and Forestry University, Fuzhou, Fujian Province, CN 350002, People's Republic of China

<sup>2</sup>College of Physics and Information Engineering, and Institute of Micro-Nano Devices & Solar Cells, Fuzhou University, Fuzhou, Fujian Province, CN 350108, People's Republic of China

<sup>3</sup>Department of Energy Engineering, Hanyang University, Seoul, CN 04763, South Korea

✉ E-mail: sycheng@fzu.edu.cn

Published in Micro & Nano Letters; Received on 29th June 2017; Revised on 23rd September 2017; Accepted on 12th October 2017

In this work, an intermediate layer of Mo is pre-deposited on the flexible Mo foil before the deposition of  $\text{Cu}_2\text{ZnSnS}_4$  (CZTS) thin film to optimise the characteristics of the flexible CZTS thin film solar cell (TFSC). It is confirmed that the pre-deposition of the Mo layer leads to the improvement in the degree of the interface matching between the back electrode and the CZTS thin film which is always regarded as the main recombination centres of the carriers in the solar cell. By employing a Mo interlayer between the Mo foil and CZTS layer, the conversion efficiency of the as-fabricated (Mo foil/Mo/CZTS/CdS/i-ZnO/AZO/Ni/Al) solar cell is further increased from 1.27 to 1.46%. Meanwhile, the traditional structure (soda-lime glass/Mo/CZTS/CdS/i-ZnO/AZO/Ni/Al) CZTS TFSC acted as a matched group which is also prepared and obtained a conversion efficiency of 1.58%. This work demonstrates for the first time the effects of Mo intermediate layers in the flexible CZTS TFSCs.

**1. Introduction:** A kesterite  $\text{Cu}_2\text{ZnSnS}_4$  (CZTS) compound semiconductor has attracted increasing attention and emerged as a promising candidate for absorber materials in thin film solar cell (TFSC) field because of its *p*-type conductivity, appropriate direct bandgap ( $\sim 1.5$  eV) and high absorption coefficient ( $\geq 10^4 \text{ cm}^{-1}$ ) [1–3]. In addition, it can also be regarded as an alternative to  $\text{CuInS}_2$  and  $\text{Cu(In,Ga)Se}_2$  absorbers, in which the extremely expensive and limited indium resource is replaced by the abundant, low cost zinc (Zn) and tin (Sn). The CZTS TFSCs coated on the soda-lime glass (SLG) substrate has made great progress. The  $\text{Cu}_2\text{ZnSn(S,Se)}_4$  solar cells displayed the highest conversion efficiency of  $12.6 \pm 0.3\%$  and the highest conversion efficiency of 9.26% for pure phase CZTS TFSCs [4]. However, the conversion efficiency is far from the theoretical efficiency of 32.2% for CZTS TFSCs [5]. Also, the CZTS TFSCs on flexible substrates seem to be more attractive for the applications on both ground and space utilities due to their high power/mass (W/kg) ratios, as well as further cost reduction by the roll-to-roll deposition method [6, 7]. Compared with other flexible substrates (stainless steel, aluminium, and organic films), flexible molybdenum foil has attractions of its own, such as high temperature resistance, good mechanical strength, the compatible coefficient of linear thermal expansion. Additionally, molybdenum is the first choice for its compatible coefficient of linear thermal expansion (linear CTE),  $5.2 \times 10^{-6} \text{ K}^{-1}$  [8]. Besides, the high purity molybdenum foil-based cell structure is free of barrier layers, whereas other substrates such as stainless steel containing some deep level impurities like Fe, which adversely affects the electronic properties of the absorbers [9]. Furthermore, the CZTS thin films fabricated on the Mo foils exhibited good crystallinity than those on the other flexible metal substrates [10].

Currently, there are some reports about the CZTS TFSCs which were constructed on flexible molybdenum foils. For instance, Qiwen Tian and co-workers fabricated the CZTS solar cells (Al foil/Mo/CZTS/ZnS/i-ZnO/ITO/Ni/Al) by using the successive ion layer adsorption and reaction process which exhibited a power conversion efficiency of 1.94% [11]. In addition, CZTS TFSCs (Mo foil/Mo film/ CZTS/CdS/ZnO/AZO/Al) with the highest conversion efficiency up to 3.82% has been achieved in which the

CZTS thin films are prepared by an electro-deposition method [12]. Though the CZTS TFSCs have got some favourable conversion efficiencies, there are few studies on the mechanism of the promotion of the properties in Mo foil substrate-based flexible CZTS TFSCs. Promisingly, novel CZTS-based photovoltaic cells with traditional structures prepared by low cost sol-gel technique exhibited efficiencies of more than 3% in the laboratory [13], and the highest efficiency for  $\text{Cu}_2\text{ZnSn(S,Se)}_4$ -based device by the sol-gel method is about 7.5%.

In this Letter, the CZTS thin films were fabricated on the flexible Mo foils by the sol-gel process and the following sulphurisation in the atmosphere of  $\text{H}_2\text{S}$  and  $\text{N}_2$ . Then, the mechanism of the flexible CZTS TFSCs prepared on the Mo foils was systematically investigated. For comparison, the other three different kinds of the CZTS TFSCs (SLG/Mo/CZTS/CdS/ZnO/AZO/Ni/Al, Mo foil/CZTS/CdS/ZnO/AZO/Ni/Al, Mo foil/Mo/CZTS/CdS/ZnO/AZO/Ni/Al) were also created and the *J-V* characteristics of the CZTS solar cells in the light were then evaluated. The effects of Mo intermediate layers on the flexible CZTS TFSCs were investigated. To the best of our knowledge, there are rare reports of the effects of the Mo intermediate layers on the flexible CZTS thin film solar cells.

**2. Experiment details:** SLG, Mo foil, and Mo foil/Mo were employed as the substrates to fabricate CZTS solar cells. Firstly, in order to gain a clean surface,  $2.5 \text{ cm} \times 2.5 \text{ cm}$  SLG substrates were treated by ultrasonic cleaning in acetone and alcohol bath, each for 15 min. Secondly, the surface of the Mo foil (0.02 mm thick, 99.99% purity) was cleaned and polished at 6 V (versus Ag/AgCl) at room temperature for 1.5 min in a mixed solution of 87.5 ml methanol and 12.5 ml sulphuric acid [12]. Then, the CZTS precursor sol solution was coated on the Mo foil by using a spin-coating technique. The thickness of the CZTS thin film can be controlled only by repeating the above process. Sol-gel precursor solutions are prepared by continually dissolving copper(II) acetate monohydrate, zinc acetate dihydrate, tin(II) chloride dihydrate, and thiourea into the mixed solution of 25 ml of 2-methoxyethanol and 1 ml of triethanolamine.

Triethanolamine acted as a stabiliser and chelating agent to increase the stability of the ion complex. Sol-gel solutions were spin-coated at a speed of 2500 rpm for 30 s on the Mo foils, which are then dried in air at 250°C for 5 min to remove the residual organic materials. Then the precursors were sulphurised in an  $N_2 + H_2S$  (5%) gas atmosphere at 500°C for 90 min to obtain the fine CZTS thin films with the ratio of elementary composition fitting Cu-poor and Zn-rich conditions and the desired film thickness (about 1–2  $\mu m$ ) [14]. Fig. 1a shows the homogeneous sol-gel solution with bright yellow colour. The resulting CZTS thin film was immersed in deionised water for 10 min for removing the oxidation phase. Fig. 1b shows the prepared solar cells. To fabricate the CZTS TFSC, a CdS buffer layer, i-ZnO, AZO layers and Ni–Al electrodes were deposited, subsequently with details described elsewhere (the structure of the flexible CZTS TFSCs is shown in Fig. 2) [15]. To study the influences of the Mo interlayer on the flexible CZTS TFSC, a Mo layer of 500 nm thickness was sputtered on the Mo foil. Also, the traditional structure CZTS TFSCs with SLG substrates were used as the control group samples for the study.

The film thickness was measured by a stylus profiler (TENCOR D100). The crystallinity of the CZTS thin films was investigated by X-ray powder diffraction (XRD, Cu target,  $\lambda = 1.5406 \text{ \AA}$ , 40 kV, 30 mA) and Raman spectroscopy (RENISHAW) techniques with 532 nm excitation wavelength. The morphology and composition analyses were carried out using a scanning electron microscopy (SEM) (Nova Nano SEM 230) equipped with an Energy Disperse Spectroscopy (EDS) attachment and transmission electron microscopy (TEM) (TECNAI G2F20). The oxidation states of all the elements in the CZTS nanoparticles were confirmed by X-ray

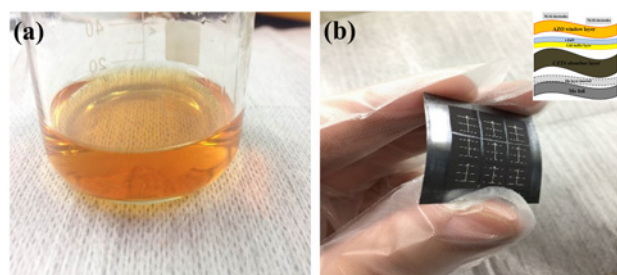
photoelectron spectroscopy (XPS) analysis (ESCALAB 250). The measured transmittance excluded scattering light. The bandgap was calculated from the experimental transmission and reflection data. The electrical properties of the absorbers were evaluated using an HMS-3000 Hall measurement system. Photo energy conversion characterisation was performed by using a source meter (Model 2400, Keithley Instruments Inc., USA) under an illumination intensity of  $100 \text{ mW/cm}^2$  (Oriel 91192, AM1.5, Global). The external quantum efficiency (EQE) measurement was carried out to study the characteristics of the different CZTS TFSCs.

### 3. Results and discussions

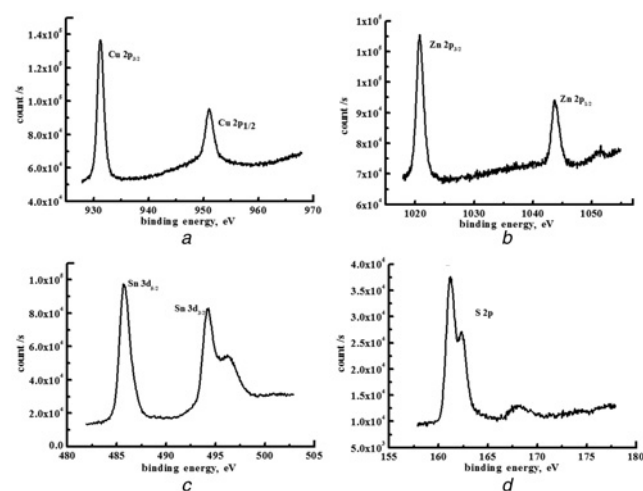
**3.1. Characteristics of CZTS thin films:** From the standard Energy Dispersive X-ray Spectroscopy (EDX) profiles of the CZTS thin film, we can know that the optimal atomic ratios of the CZTS thin film are  $Cu/(Zn + Sn) = 0.87$  and  $Zn/Sn = 1.15$ . Also from the previous study, we conclude that the ratios are the optimal compositional ratios in CZTS thin films which are similar to the other groups' experimental results [15–20]. It is noticed that the Cu-poor/Zn-rich composition can promote the  $V_{Cu}$  and  $Zn_{Cu}$  to become the dominant defects in the CZTS defect system and the  $V_{Cu}$  and  $Zn_{Cu}$  are the dominant  $p$ -type acceptors in CZTS samples [21]. As shown in Figs. 2a–d, XPS is employed to determine the stoichiometries and oxidation states of the elements of the CZTS sample. The peak of Cu 2p splits into 930.70 ( $2p_{3/2}$ ) and 950.55 eV ( $2p_{1/2}$ ) and a peak splitting of 19.85 eV indicates Cu(I) (Fig. 2a). The peaks of Zn 2p at 1044.9 and 1021.8 eV suggest the presence of Zn(II) with a peak splitting of 23.1 eV (Fig. 2b). From Fig. 2c, the Sn 3d<sub>5/2</sub> and 3d<sub>3/2</sub> peaks at 486.5 and 495 eV with a peak splitting of 8.5 eV confirm the Sn(IV) state. The S(2p) peaks are located at 160.57 and 161.72 eV, which match well with the 160–164 eV range of S in the sulphide phases (Fig. 2d). XPS results confirm the phase purities of the CZTS samples.

Fig. 3a displays the XRD patterns of the CZTS film. The CZTS film is a polycrystalline film and has a kesterite structure with XRD peaks corresponding to (112), (200), (220) and (312) reflections [22, 23]. From Scherrer's formula, the average grain size of the film is around 180 nm. From the surface analysis, as shown in Fig. 3b, there are large clumpy granules on the surface of the CZTS film, which are loosely packed together and form a continuous network. Moreover, it is clear to see that the CZTS thin film presents an analogous surface morphology.

Furthermore, as shown in Fig. 4, the morphology of the as-synthesised CZTS material is investigated by TEM. Fig. 4a shows that the particle size is about 1  $\mu m$ , which is corresponding to the above result as shown in Fig. 3b. Figs. 4b and c are the high-resolution TEM (HRTEM) and selected area electron diffraction (SAED), respectively. The HRTEM images confirm the single crystalline nature of the as-synthesised CZTS absorber materials with high qualities. The lattice fringes of CZTS materials with an interplanar spacing of 0.311 nm is ascribed to the (112) plane of kesterite CZTS. The SAED patterns of a random region of CZTS materials verify that the sample has a tetragonal structure, which



**Fig. 1** The images of CZTS gel solution and the flexible CZTS TFSC  
a Homogeneous sol-gel solution with bright yellow colour  
b Device picture of the CZTS TFSC



**Fig. 2** XPS graphs of the CZTS thin film  
a Cu element  
b Zn element  
c Sn element  
d S element

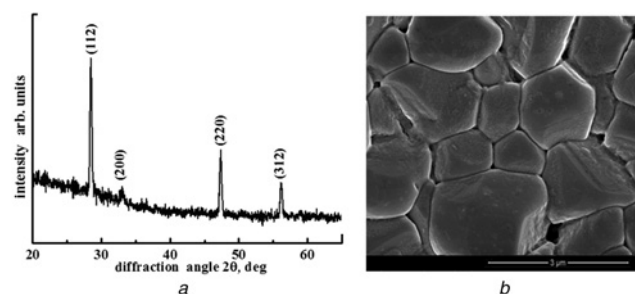


**Fig. 3** The structure characteristics of the CZTS thin film  
a XRD pattern of the CZTS thin film  
b SEM graph of the CZTS thin film

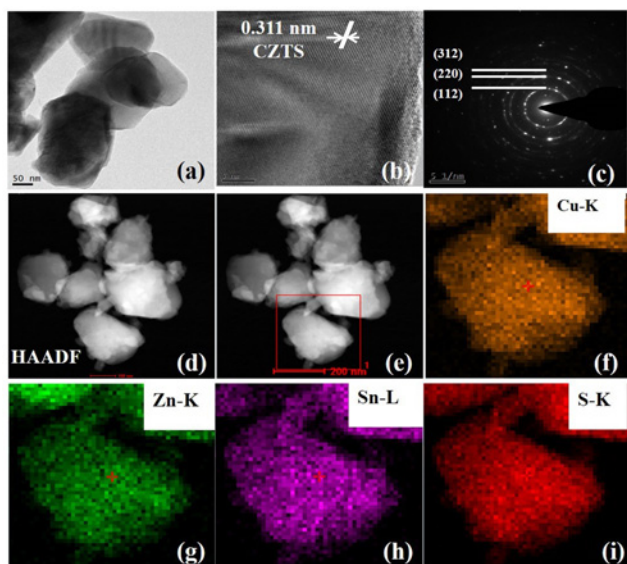


**Fig. 4** The TEM and STEM images of the as-synthesised CZTS materials  
a–c TEM pictures of the morphologies about the as-synthesised CZTS materials  
d–i STEM elemental mapping of the CZTS materials

is consistent with the above XRD results. To identify the elemental distributions and composition of CZTS materials, we perform the scanning TEM (STEM) elemental mapping to confirm the homogeneity of the chemical composition. Chemical analyses with very high spatial resolution are conducted. The selected area is scanned through the sample to detect different elements including Cu, Zn, Sn, and S, respectively. The 2D-projected chemical mappings for the four elements are presented in Figs. 4d–i. On the one hand, the CZTS material has the uniform composition distribution. On the other hand, the quantitative calculations from an EDS equipped within the STEM instrument shows the ratios of  $\text{Cu}/(\text{Zn} + \text{Sn}) = 0.87$  and  $\text{Zn}/\text{Sn} = 1.15$ . It implies that Cu-poor and Zn-rich compositions in the CZTS thin film samples. It suggests that the uniform CZTS material could be produced through the sol-gel method. Figs. 5a and b show that the absorption rate and  $E_g$  of the deposited CZTS thin films. The results match with those reported in Ref. [24–27].

To study the effect of the Mo intermediate layer on the CZTS thin films with flexible Mo foil substrates, the XRD patterns and Raman spectra of the CZTS thin films with different flexible substrate structures are shown in Fig. 6. From Fig. 6a, it is found that the CZTS film is a polycrystalline film and has a kesterite structure with XRD peaks corresponding to (112), (200), (220) and (312) reflections. When the Mo layer is inserted, the intensity of the (112) preferred orientation increases but the intensity of the peak about  $\text{MoS}_2$  decreases from Fig. 6a. Moreover, from the inserted pattern of

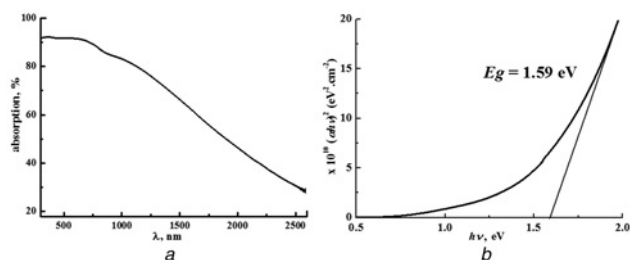


**Fig. 5** The optical properties of the deposited CZTS thin films  
a Absorption band gap of the deposited CZTS thin films  
b Energy band gap of the deposited CZTS thin films

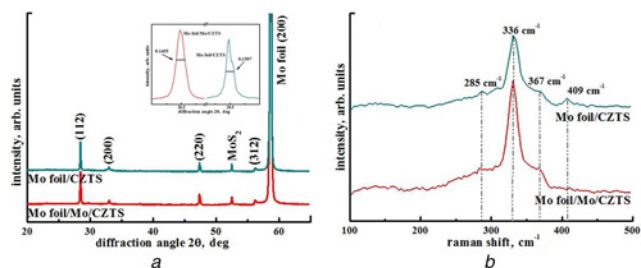


**Fig. 6** The structure characteristics of CZTS thin films with different substrate structures  
a XRD patterns of the deposited CZTS thin films with different substrate structures inserted with the XRD intensity of the CZTS (112) main peak and corresponding FWHM  
b Raman spectra of the deposited CZTS thin films with different substrate structures

Fig. 6a, it also shows that the values of full width at half maximum (FWHM) of the main peak (112) decreases when the Mo layer is inserted, which infers that the better crystallinity when the Mo layer is inserted between the CZTS thin film and Mo foil. This result is in agreement with the favourable average grain size and surface morphology observed in the surface images as shown in Fig. 7. Fig. 6b shows that the Raman spectra of the CZTS film with a 532 nm excitation wavelength. Three peaks at 285, 336 and 367  $\text{cm}^{-1}$  match with the Raman spectroscopy of the CZTS in the other reports [28–31]. The peak at 409  $\text{cm}^{-1}$  is attributed to the  $\text{MoS}_2$  [32]. It shows that with the Mo layer inserted, the intensity of  $\text{MoS}_2$  decreases and the intensity of the major peak (336  $\text{cm}^{-1}$ ) of the CZTS increases and it infers that the Mo intermediate layer could improve the crystallinity of the CZTS and inhibited the growth of  $\text{MoS}_2$  but not eliminate the presence of  $\text{MoS}_2$  completely. Also, the results could also be proved from Fig. 7.

The Hall Effect measurement shows that the as-grown CZTS film is of *p*-type conduction ( $\rho = 6.38 \Omega \text{ cm}$ ,  $\mu = 12.04 \text{ cm}^2/(\text{V s})$ ,  $p = 8.23 \times 10^{16} \text{ cm}^{-3}$ ), and the band gap of the film is around 1.59 eV. The optical band gap and electrical values of our CZTS samples can meet the requirement of the absorbing layer of the solar cell [33–44].

**3.2. Solar cell analysis:** Besides the absorbing layer (CZTS), the solar cell includes buffer layer CdS film ( $\sim 50 \text{ nm}$ ), *i*-ZnO film ( $\sim 50 \text{ nm}$ ) intrinsic layer & window layer Al-doped ZnO (AZO) ( $\sim 135 \text{ nm}$ ) film and Ni/Al metal grids ( $\sim 50/800 \text{ nm}$ ) which were fabricated by chemical bath deposition, radiofrequency magnetron sputtering and thermal evaporation, respectively. Moreover, the Mo interlayer thin film of the flexible CZTS TFSC was prepared by sputtering and the thickness is about 500 nm. Finally, the cell area of 0.25  $\text{cm}^2$  is obtained by a mechanical scribing step. The insert photo in Fig. 1b shows the whole structure of the flexible CZTS TFSC. The traditional structure CZTS TFSC which is constructed under the same condition is used for reference.

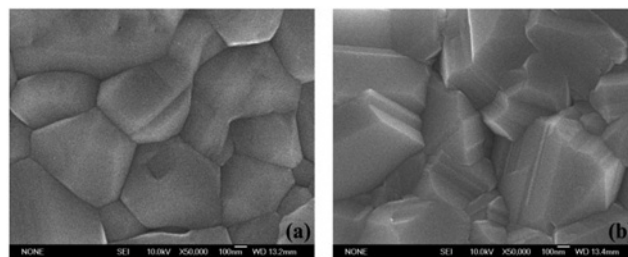


**Fig. 7** SEM graphs of the CZTS thin films on the Mo foils  
a Without Mo layer  
b With Mo layer



Fig. 7 shows the SEM images of the CZTS thin films coated on the Mo foils. Obviously, the Mo film is inserted between the Mo foil and the CZTS film. Meanwhile, the particle edge location of the CZTS thin film becomes sharper than that of the CZTS thin film which is deposited on the Mo foil directly. This can improve the carrier transport capacity and further influence the Ohmic contact characteristics of the interface between the absorber layer and the back electrode. It may be due to the fact that when the particle edge becomes sharper, the particle contact area decreases, in other words, the grain boundaries decrease and it makes the minor carrier life increase. Table 1 shows the electrical properties of CZTS thin films with and without the Mo intermediate layer on Mo foils and it shows that with the Mo intermediate layer inserted, the mobility of the CZTS thin film increases and prove the results of Fig. 7. Otherwise, the sharper particle can decrease the defects between the back contact layer and CZTS thin film. Also it can improve the interface contact and further decrease the series resistivity of the CZTS TFSCs proved in Table 2. These results identify that the Mo film interlayer not only affects the Ohmic contact characteristics between the CZTS thin film and the back electrode but also influence the morphology of the CZTS thin film.

Figs. 8a and b show the  $J-V$  curves and EQE of the CZTS TFSCs with different substrates. It can be seen that the conversion efficiency of the CZTS TFSC coated on the Mo foil is the lowest. After sputtered a thin layer of Mo on the Mo foil, both the conversion efficiency of the CZTS TFSC and the  $V_{OC}$  are improved besides the  $J_{SC}$  is decreased. This may be due to the  $MoS_2$  which is produced through the chemical reaction of the Mo interlayer and the  $H_2S$  during the sulphurisation process. The thick  $MoS_2$  layer can result in high resistance, thus decrease the  $J_{SC}$  of the CZTS TFSC [45, 46]. In Table 1, it also shows that when the substrate is Mo foil, the series resistance increases sharply due to the interface defect because of the Mo foil mechanical bending.

**Table 1** Electrical parameters of CZTS thin films with and without Mo intermediate layer

Substrate	$p$ , $cm^{-3}$	$\mu$ , $cm^2/(V\ s)$	$\rho$ , $\Omega\ cm$
Mo foil	$1.01 \times 10^{17}$	11.99	4.89
Mo foil/Mo	$5.98 \times 10^{16}$	14.32	7.02

**Table 2** Electrical parameters of the traditional and flexible structure CZTS TFSCs

Substrate	$\eta\%$	FF	$V_{OC}$ , mV	$J_{SC}$ , $mA/cm^2$	$R_s$ , $\Omega\ cm^2$
SLG/Mo	1.58	0.44	380	9.55	8.24
Mo foil	1.27	0.30	290	14.67	11.28
Mo foil/Mo	1.46	0.43	360	9.52	8.44

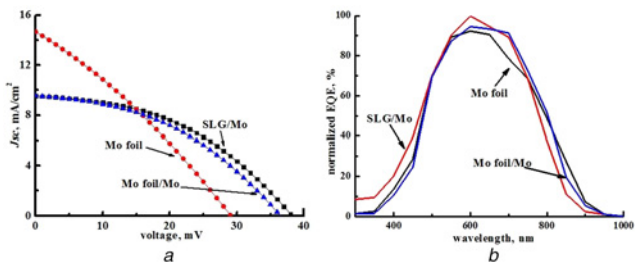


**Fig. 8** The  $J-V$  and EQE characteristics of the CZTS TFSCs with different substrate structures in light conditions  
a  $J-V$  curves of the CZTS TFSCs with different substrates  
b EQE of the CZTS TFSCs with different substrates

After sputtering an intermediate Mo, the series resistance decreases. It is suggested that the crystallisation of the modified CZTS thin films is improved and the interface recombination centre is reduced due to the Mo film. To observe the damage mechanism of the CZTS TFSCs on different substrates, we use the EQE tests to analyse the CZTS TFSCs with different structures and then normalisation processing is carried out as shown in Fig. 8b. The EQE test result shows that the light response of the solar cells under different wavelengths of incident light. From Fig. 8b, firstly in the range of short wavelength light ( $>2.4\ eV$ , the  $E_g$  of CdS), with the increasing of the wavelength, the photo-response curves of the three kinds of structure CZTS TFSCs increase obviously. It suggests that the light in the range of the short wavelength is absorbed by CdS films. However, there is hardly any improvement in the short wavelength region due to the absorption loss in the buffer layer. However, when the light wavelength is above 600 nm, the relatively higher spectral response of the modified samples with the Mo intermediate layer is observed. It indicates a low recombination rate at the interface between the back electrode and CZTS thin film. It can be found that several groups of solar cells with different substrate structures have been fabricated and proved that the above effects on the performance can be repeated. However, in the range of the red light band, it shows that the CZTS TFSC has a better optical response than the flexible CZTS TFSCs. Fig. 9 shows the dark  $J-V$  curves of the CZTS TFSCs with different substrates. When the Mo layer is inserted, the reverse saturation current of the flexible CZTS TFSC is smaller than that of flexible CZTS TFSC without the Mo layer. It may be mainly due to the fact that when the Mo layer inserted between the Mo foil and CZTS thin film, the defects of the interface between them decrease and then the reverse saturation current which arose from the tunnelling effect decreases. Moreover, because of the defects of Mo foil bending about flexible CZTS TFSCs, the traditional structure CZTS TFSC has the lowest reverse saturation current.

The cross-sectional SEM photos of the corresponding CZTS solar cells are shown in Fig. 10 and the energy band diagrams of the flexible CZTS TFSC on different substrates are shown in Fig. 11. They show that the growth of  $MoS_2$  was restrained with the Mo interface layer and the degree of the interface matching between the back electrode and CZTS thin film is improved

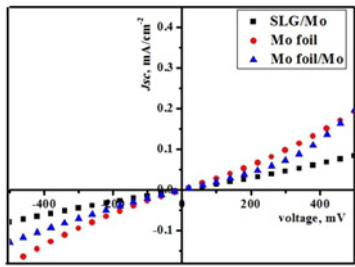


**Fig. 9** Dark  $J-V$  curves of the CZTS TFSCs with different substrates

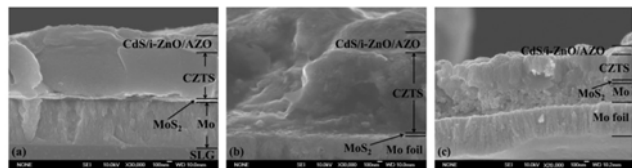


**Fig. 10** SEM cross-section diagram of the CZTS TFSCs on different substrates  
a SLG/Mo  
b Mo foil  
c Mo foil/Mo

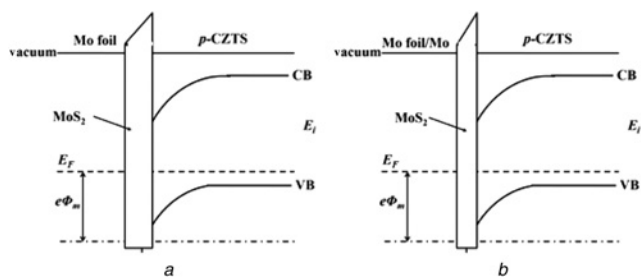


**Fig. 11** Energy band diagrams of the flexible CZTS TFSC on different substrates  
a Mo foil  
b Mo foil/Mo

apparently which accordingly decreases the interface defects. Therefore the opportunity of recombination at the interface is reduced.

From the analysis of the CZTS TFSCs, it infers that the flexible CZTS TFSCs obtain conversion efficiency, but the efficiency is lower than that of the traditional structure CZTS TFSC. This may be due to the intrinsic mechanical properties of the Mo foil that the Mo is easy to bend and the following performance of the CZTS TFSC is easy to be broken. It is caused by the two following reasons: one is that the bend of the flexible Mo foil leads to the damage of the structure of the cells and then decreases the light absorption ability; the other one is that the introduction of the impurities through the sulphurisation process leads to the increase of the defects in the CZTS thin films, which increases the recombination probability of the minority carriers and decreases the generation of the photocurrent.

**4. Conclusion:** The CZTS TFSCs with kesterite structure CZTS thin films coated on different substrates are prepared by an environmental sol-gel method and the following sulphurisation process. After sulphurisation, highly compact CZTS thin films with significant grain growth and fine electrical property are obtained. By employing a Mo interlayer between the Mo foil and CZTS layer, the conversion efficiency of the as-fabricated (Mo foil/Mo/CZTS/CdS/i-ZnO/AZO/Ni/Al) solar cell is further increased from 1.27 to 1.46%. After inserting a sputtering Mo film on the Mo foil, both the conversion efficiency of the CZTS TFSC and the  $V_{OC}$  are improved though the  $J_{SC}$  is decreased. It is indicated that the Mo film decreased the defect centre and improved the characteristics of the Ohmic contact between the absorber layer and Mo film. Based on the above analysis, it can be concluded that these flexible CZTS TFSCs have a broad application prospect. However, the defects during the flexible substrate bending process and the following produced impurities limit the flexible CZTS TFSC energy conversion abilities. Therefore, the high performance of the flexible CZTS TFSC needs more scientific research and further development.

**5. Acknowledgments:** This research was supported by the National Natural Science Foundation of China (grant no. 61574038), and the Science Foundation of Fujian Science & Technology Department (grant nos. 2015H0021, 2015J05124 and 2016H6012)

## 6 References

- [1] Liu X., Feng Y., Cui H., *ET AL.*: 'The current status and future prospects of kesterite solar cells: a brief review', *Prog. Photovolt., Res. Appl.*, 2016, **24**, pp. 879–898
- [2] Yu K., Carter E.A.: 'Determining and controlling the stoichiometry of  $\text{Cu}_2\text{ZnSnS}_4$  photovoltaics: the physics and its implications', *Chem. Mater.*, 2016, **28**, pp. 4415–4420
- [3] Tsai H.W., Chen C.W., Thomas S.R., *ET AL.*: 'Facile growth of  $\text{Cu}_2\text{ZnSnS}_4$  thin-film by one-step pulsed hybrid electrophoretic and electroplating deposition', *Sci. Rep.*, 2016, **6**, pp. 19102–19108
- [4] Liu F., Huang J., Sun K., *ET AL.*: 'Beyond 8% ultrathin kesterite  $\text{Cu}_2\text{ZnSnS}_4$  solar cells by interface reaction route controlling and self-organized nanopattern at the back contact', *NPG Asia Mater.*, 2017, **9**, p. e401
- [5] Shockley W.: 'Problems related to p-n junctions in silicon', *Solid-State Electron.*, 1961, **2**, pp. 35–67
- [6] Gao Z., Zhao M., Zhuang D., *ET AL.*: 'Study on the performance of tungsten–Titanium alloy film as a diffusion barrier for iron in a flexible CIGS solar cell', *Sol. Energy*, 2015, **120**, pp. 357–362
- [7] Sun K., Su Z., Yan C., *ET AL.*: 'Flexible  $\text{Cu}_2\text{ZnSnS}_4$  solar cells based on successive ionic layer adsorption and reaction method', *RSC Adv.*, 2014, **4**, p. 17703
- [8] Patel M., Ray A.: 'Enhancement of output performance of  $\text{Cu}_2\text{ZnSnS}_4$  thin film solar cells – a numerical simulation approach and comparison to experiments', *Physica B*, 2012, **407**, pp. 4391–4397
- [9] Herz K., Eicke A., Kessler F., *ET AL.*: 'Diffusion barriers for CIGS solar cells on metallic substrates', *Thin Solid Films*, 2003, **431–432**, pp. 392–397
- [10] Xu J., Cao Z., Yang Y., *ET AL.*: 'Characterization of  $\text{Cu}_2\text{ZnSnS}_4$  thin films on flexible metal foil substrates', *J. Mater. Sci., Mater. Electron.*, 2015, **26**, pp. 726–733
- [11] Tian Q., Xu X., Han L., *ET AL.*: 'Hydrophilic  $\text{Cu}_2\text{ZnSnS}_4$  nanocrystals for printing flexible, low-cost and environmentally friendly solar cells', *CrystEngComm*, 2012, **14**, pp. 3847–3850
- [12] Zhang Y., Ye Q., Liu J., *ET AL.*: 'Earth-abundant and low-cost CZTS solar cell on flexible molybdenum foil', *RSC Adv.*, 2014, **4**, pp. 23666–23669
- [13] Cho J.W., Ismail A., Park S.J., *ET AL.*: 'Synthesis of  $\text{Cu}_2\text{ZnSnS}_4$  thin films by a precursor solution paste for thin film solar cell applications', *ACS Appl. Mater. Interfaces*, 2013, **5**, pp. 4162–4165
- [14] Long B., Cheng S., Zheng Q., *ET AL.*: 'Effects of sulfurization time and  $\text{H}_2\text{S}$  concentration on electrical properties of  $\text{Cu}_2\text{ZnSnS}_4$  films prepared by sol–gel method', *Mater. Res. Bull.*, 2016, **73**, pp. 140–144
- [15] Ahmed S., Reuter K.B., Gunawan O., *ET AL.*: 'A high efficiency electrodeposited  $\text{Cu}_2\text{ZnSnS}_4$  solar cell', *Adv. Energy Mater.*, 2012, **2**, pp. 253–259
- [16] Schnabel T., Löw M., Ahlswede E.: 'Vacuum-free preparation of 7.5% efficient  $\text{Cu}_2\text{ZnSn}(\text{S,Se})_4$  solar cells based on metal salt precursors', *Sol. Energy Mater. Sol. Cells*, 2013, **117**, pp. 324–328
- [17] Su Z., Sun K., Han Z., *ET AL.*: 'Fabrication of  $\text{Cu}_2\text{ZnSnS}_4$  solar cells with 5.1% efficiency via thermal decomposition and reaction using a non-toxic sol–gel route', *J. Mater. Chem. A*, 2014, **2**, pp. 500–509
- [18] Dhakal T.P., Peng C.Y., Reid Tobias R., *ET AL.*: 'Characterization of a CZTS thin film solar cell grown by sputtering method', *Sol. Energy*, 2014, **100**, pp. 23–30
- [19] Kauk M., Muska K., Altosaar M., *ET AL.*: 'Effects of sulphur and tin disulphide vapour treatments of  $\text{Cu}_2\text{ZnSn}(\text{S,Se})_4$  absorber materials for monograin solar cells', *Energy Procedia*, 2011, **10**, pp. 197–202
- [20] Sugimoto H., Hiroi H., Sakai N., *ET AL.*: 'Over 8% efficiency  $\text{Cu}_2\text{ZnSnS}_4$  submodules with ultra-thin absorber'. Conf. Record of the IEEE Photovoltaic Specialists Conf., 2012, pp. 002997–003000
- [21] Chen S., Gong X.G., Walsh A., *ET AL.*: 'Defect physics of the kesterite thin-film solar cell absorber  $\text{Cu}_2\text{ZnSnS}_4$ ', *Appl. Phys. Lett.*, 2010, **96**, 021902
- [22] Xu J., Yang Y., Cao Z., *ET AL.*: 'Preparations of  $\text{Cu}_2\text{ZnSnS}_4$  thin films and  $\text{Cu}_2\text{ZnSnS}_4/\text{Si}$  heterojunctions on silicon substrates by sputtering', *Optik – Int. J. Light Electron Opt.*, 2016, **127**, pp. 1567–1571
- [23] Safdar A., Islam M., Ahmad I., *ET AL.*: 'Quantum confinement and size effects in  $\text{Cu}_2\text{ZnSnS}_4$  thin films produced using solution processed ultrafine nanoparticles', *Mater. Sci. Semicond. Process.*, 2016, **41**, pp. 420–427
- [24] Sarswat P.K., Snure M., Free M.L., *ET AL.*: 'CZTS thin films on transparent conducting electrodes by electrochemical technique', *Thin Solid Films*, 2012, **520**, pp. 1694–1697
- [25] Maeda K., Tanaka K., Nakano Y., *ET AL.*: ' $\text{H}_2\text{S}$  concentration dependence of properties of  $\text{Cu}_2\text{ZnSnS}_4$  thin film prepared under nonvacuum condition', *Jpn. J. Appl. Phys.*, 2011, **50**, 05FB09
- [26] Schubert B.-A., Marsen B., Cinque S., *ET AL.*: ' $\text{Cu}_2\text{ZnSnS}_4$  thin film solar cells by fast coevaporation', *Prog. Photovolt., Res. Appl.*, 2011, **19**, pp. 93–96
- [27] Seol J.-S., Lee S.-Y., Lee J.-C., *ET AL.*: 'Electrical and optical properties of  $\text{Cu}_2\text{ZnSnS}_4$  thin films prepared by RF magnetron sputtering process', *Sol. Energy Mater. Solar Cells*, 2003, **75**, pp. 155–162
- [28] Chalapathy R.B.V., Jung G.S., Ahn B.T.: 'Fabrication of  $\text{Cu}_2\text{ZnSnS}_4$  films by sulfurization of  $\text{Cu/ZnSn/Cu}$  precursor layers in sulfur

- atmosphere for solar cells', *Sol. Energy Mater. Sol. Cells*, 2011, **95**, pp. 3216–3221
- [29] Fernandes P.A., Salomé P.M.P., da Cunha A.F.: 'Study of polycrystalline  $\text{Cu}_2\text{ZnSnS}_4$  films by Raman scattering', *J. Alloys Compd.*, 2011, **509**, pp. 7600–7606
- [30] Gurieva G., Guc M., Bruk L.I., *ET AL.*: ' $\text{Cu}_2\text{ZnSnS}_4$  thin films grown by spray pyrolysis: characterization by Raman spectroscopy and X-ray diffraction', *Phys. Status Solidi C*, 2013, **10**, pp. 1082–1085
- [31] Scragg J.J., Ericson T., Kubart T., *ET AL.*: 'Chemical insights into the instability of  $\text{Cu}_2\text{ZnSnS}_4$  films during annealing', *Chem. Mater.*, 2011, **23**, pp. 4625–4633
- [32] Liu F., Sun K., Li W., *ET AL.*: 'Enhancing the  $\text{Cu}_2\text{ZnSnS}_4$  solar cell efficiency by back contact modification: inserting a thin  $\text{TiB}_2$  intermediate layer at  $\text{Cu}_2\text{ZnSnS}_4/\text{Mo}$  interface', *Appl. Phys. Lett.*, 2014, **104**, p. 051105
- [33] Katagiri H., Saitoh K., Washio T., *ET AL.*: 'Development of thin film solar cell based on  $\text{Cu}_2\text{ZnSnS}_4$  thin films', *Sol. Energy Mater. Sol. Cells*, 2001, **65**, pp. 141–148
- [34] Scragg J.J., Dale P.J., Peter L.M., *ET AL.*: 'New routes to sustainable photovoltaics: evaluation of  $\text{Cu}_2\text{ZnSnS}_4$  as an alternative absorber material', *Phys. Status Solidi B*, 2008, **245**, pp. 1772–1778
- [35] Fernandes P.A., Salomé P.M.P., da Cunha A.F., *ET AL.*: ' $\text{Cu}_2\text{ZnSnS}_4$  solar cells prepared with sulphurized dc-sputtered stacked metallic precursors', *Thin Solid Films*, 2011, **519**, pp. 7382–7385
- [36] Liu F., Zhang K., Lai Y., *ET AL.*: 'Growth and characterization of  $\text{Cu}_2\text{ZnSnS}_4$  thin films by DC reactive magnetron sputtering for photovoltaic applications', *Electrochem. Solid-State Lett.*, 2010, **13**, pp. H379–H381
- [37] Ito K., Nakazawa T.: 'Electrical and optical properties of stannite-type quaternary semiconductor thin films', *Jpn. J. Appl. Phys.*, 1988, **27**, pp. 2094–2097
- [38] Tanaka T., Nagatomo T., Kawasaki D., *ET AL.*: 'Preparation of  $\text{Cu}_2\text{ZnSnS}_4$  thin films by hybrid sputtering', *J. Phys. Chem. Solids*, 2005, **66**, pp. 1978–1981
- [39] Rajeshmon V.G., Kartha C.S., Vijayakumar K.P., *ET AL.*: 'Role of precursor solution in controlling the opto-electronic properties of spray pyrolysed  $\text{Cu}_2\text{ZnSnS}_4$  thin films', *Sol. Energy*, 2011, **85**, pp. 249–255
- [40] Liu F., Li Y., Zhang K., *ET AL.*: 'In situ growth of  $\text{Cu}_2\text{ZnSnS}_4$  thin films by reactive magnetron co-sputtering', *Sol. Energy Mater. Sol. Cells*, 2010, **94**, pp. 2431–2434
- [41] Chan C.P., Lam H., Surya C.: 'Preparation of  $\text{Cu}_2\text{ZnSnS}_4$  films by electrodeposition using ionic liquids', *Sol. Energy Mater. Sol. Cells*, 2010, **94**, pp. 207–211
- [42] Yan C., Liu F., Sun K., *ET AL.*: 'Boosting the efficiency of pure sulfide CZTS solar cells using the In/Cd-based hybrid buffers', *Sol. Energy Mater. Sol. Cells*, 2016, **144**, pp. 700–706
- [43] Jimbo K., Kimura R., Kamimura T., *ET AL.*: ' $\text{Cu}_2\text{ZnSnS}_4$ -type thin film solar cells using abundant materials', *Thin Solid Films*, 2007, **515**, pp. 5997–5999
- [44] Katagiri H.: ' $\text{Cu}_2\text{ZnSnS}_4$  thin film solar cells', *Thin Solid Films*, 2005, **480–481**, pp. 426–432
- [45] Li W., Chen J., Cui H., *ET AL.*: 'Inhibiting  $\text{MoS}_2$  formation by introducing a ZnO intermediate layer for  $\text{Cu}_2\text{ZnSnS}_4$  solar cells', *Mater. Lett.*, 2014, **130**, pp. 87–90
- [46] Yang K.-J., Sim J.-H., Jeon B., *ET AL.*: 'Effects of Na and  $\text{MoS}_2$  on  $\text{Cu}_2\text{ZnSnS}_4$  thin-film solar cell', *Prog. Photovolt., Res. Appl.*, 2015, **23**, pp. 862–873